CHEMELECTROCHEM

Supporting Information

High-Throughput Mapping of the Electrochemical Properties of (Ni-Fe-Co-Ce)O_x Oxygen-Evolution Catalysts

Joel A. Haber,[a] Chengxiang Xiang,[a] Dan Guevarra,[a] Suho Jung,[a] Jian Jin,[b] and
John M. Gregoire*[a]

celc_201300229_sm_miscellaneous_information.pdf

Supporting Information

Preparation of Psuedo-Ternary Library on FTO/glass. The discrete pseudo-quaternary library was produced by first considering the 5456 unique compositions in the Ni-Fe-Co-Ce space with 3.33 at% composition steps and then extracting the 665 compositions that are within 5 at% of the planar cross section identified in Figure 1a. The complete array of samples was deposited by inkjet printing onto the FTO-coated side of a 10 cm x 15 cm glass plate at a resolution of 2880 x 1440 dpi.[3c] Four separate metal inks, of the type previously described by Fan and Stuckey,[S1] were prepared by mixing 5 mmoles of each of the Ni, Fe, Co, and Ce precursor with 0.80 g Pluronic F127 (Aldrich), 1.0 mL glacial acetic acid (T.J. Baker, Inc.), 0.40 mL of concentrated HNO_3 (EMD), and 30 mL of 200 proof Ethanol (Koptec). The metal precursors were $Ni(NO_3)_2$-$6H_2O$ (1.53 g, 99.999%, Sigma Aldrich), $Fe(NO_3)_3$-$9H_2O$ (2.14 g, ≥98% , Sigma Aldrich), $Co(NO_3)_2$-$6H_2O$ (1.46 g, 99.99%, Sigma Aldrich), and $Ce(NO_3)_3$-$6H_2O$ (2.22 g, 99.99%, Sigma Aldrich). The library of compositions was printed as a set of 1 mm x 1 mm spots on a 2 mm pitch. For Library A 7.5 nmoles of metal were deposited in each 1 mm^2 spot, while for Library B 3.75 nmoles of metal were deposited in each 1 mm^2 spot. The difference in electrochemical properties from this slight variation in synthesis procedure was found to be inconsequential for the results of this manuscript. After printing, the inks were dried and the metal precursors converted to oxides by calcination in air at 40 °C for 18 h, then at 70 °C for 24 h, followed by a 5 h ramp and 10 h soak at 350 °C.

Preparation of Three Compositions on Glassy Carbon. The three selected ***low-Ce*** , ***medium-Ce***, and ***high-Ce*** compositions ($Ni_{50}Fe_{30}Co_{17}Ce_3$, $Ni_{40}Fe_{20}Co_{20}Ce_{20}$ and $Ni_{30}Fe_7Co_{20}Ce_{43}$) were printed onto glassy carbon rotating disk electrodes (GC RDEs, SIGRADUR G, HTW Hochtemperatur-Werkstoffe GmbH), which are cylinders 5 mm in diameter and 4 mm in height. Four separate metal inks were prepared as described above and printed at 2880 x 1440 dpi, at 7.5

nmoles of metal per mm^2, as in Library A. After printing, the inks were dried and the metal precursors converted to oxides using the same calcination and annealing process used for the combinatorial library.

Electrochemical Characterization

Scanning droplet photoelectrochemical cell.

The detailed geometry and operational performance of a scanning droplet cell were described by Gregoire, et. Al.[3b] Briefly, a drop of solution was formed on top of a 1 mm x 1 mm ink-jet printed sample. The shape of the droplet was directed and controlled by a solution inlet port and multiple solution outlet ports without the need for a sealing gasket. The scanning droplet cell (SDC) provided an individual 3-electrode cell for each sample, including a capillary Ag/AgCl reference electrode terminating within 1 mm of the sample surface and a platinum wire counter electrode placed in the solution influent. In this study, we continuously supplied an oxygen-saturated 1.0 M NaOH(aq) solution to form a drop contact to each catalyst sample, which in this SDC configuration produces an R_u = *ca.* 15 Ω. After moving to a new sample location, a 2 second cell stabilization period preceded the electrochemical experiments, which for Library A included a series of CP measurements at current densities J = 10, 1 and 19 mA cm^{-2}. The durations of the experiments was chosen to be 15, 20, and 4 s, respectively to ensure that quasi-steady state behavior was attained. The catalyst overpotential η was determined by averaging the measured potential over the final 1 s for each current density, creating the compositional maps of catalyst performance shown in Figures 1b-1d. A similar series of CP measurements was performed on Library B (data not presented here) followed by a CV at 100 mV s^{-1} from -50 mV to 450 mV overpotential for the OER reaction. This CV data was used for analysis of sample redox behavior, as described below.

Electrochemical analysis of catalysts on glassy carbon rotating disk electrodes. GC RDE electrodes coated with each composition were subjected to a series of electrochemical measurements in oxygen-saturated 1.0 M NaOH blanketed under 1 atm O_2(g). The working electrode was rotated at 1600 rpm and the counter and reference electrodes were a carbon rod (99.999%, Alfa Aesar), and a commercial saturated calomel electrode (SCE) (CH-Instruments), respectively.

All measurements were conducted in a modified two-chamber U-cell in which the first chamber held the working and reference electrodes in *ca.* 120 mL of solution, and the second chamber held the auxiliary electrode in *ca.* 25 mL. The two chambers were separated by a fine-porosity glass frit. The cell was purged for *ca.* 20 min with O_2 prior to each set of experiments. During static-voltammetry measurements, the solution in the first chamber was blanketed under O_2. During rotating-disk electrode voltammetry measurements, the solution in the first chamber was continuously bubbled with O_2. The uncompensated resistance of the cell was measured with a single-point high-frequency impedance measurement and IR drop was compensated at 85% through positive feedback using the Bio-Logic EC-Lab software. The typical electrochemical cell had R_u = *ca.* 20 Ω in 1 M NaOH. Each catalyst was investigated by a CV at 10 mV s^{-1} (forward sweep shown in Figure 2), a series of 30 second controlled-current CP steps and a series of controlled-potential CA steps.

In the low-η region of the CVs in Figure 2, the oxidative currents deviate from the pure exponential trend due to the reversible oxidation of the catalyst film, particularly for the low-Ce composition. The quasi-steady state CP and CA measurements in Figure 2 do not contain appreciable sample oxidation current and thus follow the Tafel trend. At high-η the data deviate from the exponential behavior due to bubble formation at the electrode surface and corresponding decrease in electrochemically accessible surface area.

Method of Extracting Reversible Red-Ox of the Catalyst Film from Cyclic Voltammetry

The CV data collected from the pseudoternary library on FTO/glass using the SDC was analyzed by fitting the forward sweep and reverse sweep separately. To reveal the signals arising from the reversible redox processes occurring in the catalyst film, the current-potential data was fit with two components which were then subtracted: (1) a linear fit to capacitive and residual currents, and (2) an exponential fit the catalyzed oxygen evolution reaction.

Example curve fittings are shown in Figure S1 for the oxidative forward sweep for the three compositions ($Ni_{50}Fe_{30}Co_{17}Ce_3$, $Ni_{40}Fe_{20}Co_{20}Ce_{20}$ and $Ni_{30}Fe_7Co_{20}Ce_{43}$). The inset of Figure S1a shows the signals for the reversible oxidative process occurring in the catalyst film after subtraction of the linear background and exponential catalytic OER components. Integration of the peak areas of the remaining reversible oxidation process yields the charge extracted from the catalyst film. Figure S1b maps this sample charging as a function of composition for the entire pseudoternary library. The average oxidation potential for the reversible oxidation of the catalyst film was calculated as described in the paper. Figure S1c plots both the oxidative charge of catalyst film and the average potential at which this process occurred as a function of composition along the pseudobinary line shown in Figure 3a.

Figures S1a and b both indicated that charge transferred to the film was greater at the intermediate Ce concentrations. Assuming a 1 e- reaction, the reaction charge shown in Figures S1a and b corresponds to the oxidation of 2-15% of the 3.75 nmol of metal in the sample. Since the oxidation charge does not vary monotonically with any composition direction, the identification of the cations being oxidized and the nature of the oxidation process require further investigation.

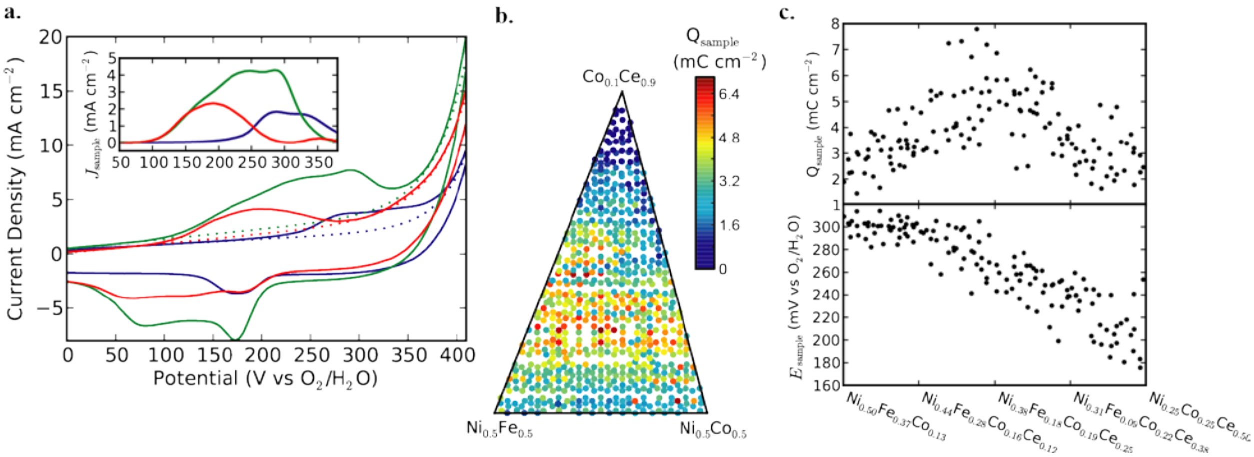

Figure S1. a) Illustrative curve fitting to the oxidative forward sweep of the CV for the compositions $Ni_{50}Fe_{30}Co_{17}Ce_3$ (blue), $Ni_{40}Fe_{20}Co_{20}Ce_{20}$ (green), and $Ni_{30}Fe_7Co_{20}Ce_{43}$(red), with the inset showing the resulting current signal arising from oxidation of the catalyst film. b) Composition map of the integrated charge extracted from the catalyst film over the pseudoternary library, Q_{sample}. c) Plots of Q_{sample} and average potential for the oxidation of the catalyst film (E_{sample}) as a function of composition across the pseudobinary line.

It is important to note that the extraction of Tafel slope from the electrochemical measurements does not involve identification of an equilibrium potential. When using Tafel analysis to study catalyst mechanism, an equilibrium potential is defined and the Tafel slope extrapolation of the high-η catalytic current to the equilibrium potential provides the exchange current density. For multi-step reactions such as OER, the likely presence of a rate determining step confounds the application of this simple model. However, it is still useful to observe composition trends in an extrapolated current density, in particular because the Tafel slope varies so significantly. To this end, we use the extrapolation method described above to calculate a nominal current density.

Using the Tafel fit of the high throughput CP data, $J_{O2/H2O}$ is the current density extrapolated to the O_2/H_2O equilibrium potential (see Figure 2), which is shown as a function of composition in Figure S2a. For comparison the map of Tafel slope (same as Figure 4b) is shown in Figure S2b. The anti-correlation of $J_{O2/H2O}$ and α conspire to yield the engineering figure of merit trends shown in Figure 1. Figure S2a indicates that the newly discovered catalyst exhibits a 1000-fold increase in the nominal exchange current.

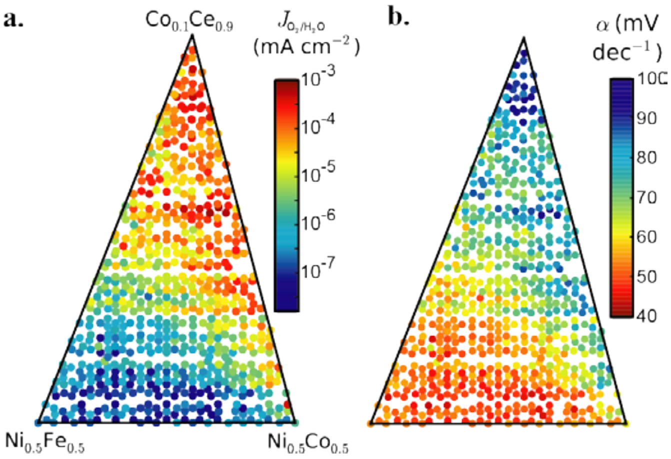

Figure S2. a) Map of a nominal Tafel-extrapolated current density (see text) and b) map of the Tafel slope extracted from the CP data displayed in Figure 1.

From the point of view of surface area engineering described in the manuscript, this great increase in current density of the high-Ce catalyst composition may be exploited at low overpotentials with an appropriately engineered electrode. Because the effective exchange current density, $J_{O2/H2O}$, and Tafel slope are anti-correlated with composition, the two active catalyst composition regions require similar overpotentials at the current density applicable to distributed photoelectrochemical water splitting, 10 mA/cm^2. It is due to this coincidence that the Ce-rich composition with higher Tafel slope shows the greater promise for reducing the overpotential at 10 mA/cm^2, by engineering increased catalyst surface area.

Notes on Variation in Tafel slope

Since determining the Tafel slope for a given catalyst and reaction requires measurement over a broad range of current density, uncompensated resistance can alter the apparent Tafel slope. While we are unable to measure the resistivity of each sample in the composition library, the uncompensated resistance of the scanning droplet cell itself is below 20 Ohms.[3b] For the three samples prepared on glassy carbon rods and measured using conventional RDE techniques, the total cell resistance over multiple samples was between 5 and 25 Ω, and was uncorrelated to the film composition. These are typical values for the electrochemical cell (20 Ω, see above) and suggest that the resistance of the catalyst is not appreciable and does not vary strongly in the composition range discussed in this communication.

Additional experiments were performed to demonstrate that our noted variation in Tafel slope as a function of composition is due to a fundamental change in the catalysis rather than a composition-mediated microstructural change to the well-known Ni-Fe oxide catalysts. For the representative compositions of the transition metal-rich and Ce-rich catalyst regions, CVs were acquired on an inkjet-printed library similar to Library B, described above. Using the fitting routines described above, the catalytic current was extracted for the ***low-Ce*** and ***high-Ce*** compositions, as shown in Figure S3. This plot makes it clear that the η-J curves for these specific catalyst films cross at approximately 11 mA/cm^2 and $\eta = 410$ mV. At η less than 410 mV, the ***high-Ce*** catalyst has a higher Tafel slope and produces a larger geometric current density than the ***low-Ce*** catalyst.

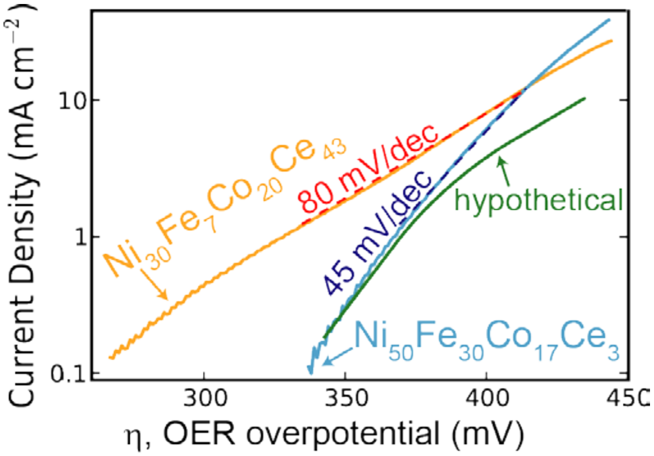

Figure S3. Catalytic current extracted from CV data is shown for the ***high-Ce*** (yellow) and ***low-Ce*** (blue) compositions. The superimposed dashed lines have the characteristic Tafel slopes for the respective composition regions (80 mV/decade for ***high-Ce*** and 45 mV/decade for transition metal-rich, ***low-Ce***). The experimental current/voltage curves are linear with the characteristic Tafel slopes for more than 1 decade of current below the cross-over point of the current-voltage curves. A hypothetical current-voltage curve for the ***low-Ce*** catalyst as it would be altered by high film resistivity is shown (green) to illustrate that the current-voltage behavior of the newly discovered ***high-Ce*** catalyst is not re-produced by physical or electrical modification of the ***low-Ce*** catalyst.

It has been demonstrated via theoretical predictions and experiments that catalyst film microstructure and catalyst layer resistance can cause the measured Tafel slope to increase to a maximum of twice the mechanistically expected value for the multi-electron ORR reaction.[S2] If the composition dependent changes in Tafel slope reported here resulted primarily from increases in film resistance with increasing Ce content, then the primary effect would be to increase the observed Tafel slope from the 45 mV/decade value of the Fe-Ni catalysts up to a maximum value of 90 mV/decade. In this case, the “modified”, more resistive ***low-Ce*** catalyst would have the same η-J relationship at low current densities and the Tafel slope would increase at larger current density. A hypothetical η-J curve for a “modified Ni-Fe”, resistive catalyst is shown (green) in Fig. S3. While this hypothetical data matches the Tafel slope of the ***high-Ce*** catalyst at high current density, the behavior of the ***high-Ce*** catalyst is markedly different from this hypothetical case. The current density of this hypothetical “modified” catalyst never exceeds that of the ***low-Ce*** catalyst, the newly discovered ***high-Ce*** catalyst has significantly larger current density at low overpotentials. Therefore, the observed η-J behavior of the ***high-Ce*** catalyst cannot result simply from an increase in the catalyst film resistivity.

In order to “modify” the ***low-Ce*** catalyst to reproduce the ***high-Ce*** η-J curve, the number of catalytically active sites would have to increase as a function of composition (increase with increasing Ce content), thereby increasing the exchange current density. The electrochemically active surface area increased by less than a factor of two—below the error in the measurement—between the ***low-Ce*** and ***high-Ce*** catalyst compositions. To create the ***high-Ce*** performance at low-η using the “active site” from the ***low-Ce*** catalyst, the surface density of the active site would have to increase by a factor of more than 10^3, and this is highly unlikely given the comparable electrochemically accessible surface areas and the approximately 50% Ce concentration in the ***high-Ce*** catalyst. The most straightforward conclusion is that the new ***high-Ce*** is a fundamentally different and its OER mechanism requires further investigation.

Additional References

[S1] a) J. Fan, S. W. Boettcher, G. D. Stucky, *Chem. Mater.* **2006**, *18*, 6391-6396; b) X. N. Liu, Y. Shen, R. T. Yang, S. H. Zou, X. L. Ji, L. Shi, Y. C. Zhang, D. Y. Liu, L. P. Xiao, X. M. Zheng, S. Li, J. Fan, G. D. Stucky, *Nano Lett.* **2012**, *12*, 5733-5739.

[S2] a) D. W. Banham, J. N. Soderberg, V. I. Birss, *J. Phys. Chem. C* **2009**, *113*, 10103-10111; b) J. N. Soderberg, A. C. Co, A. H. C. Sirk, V. I. Birss, *J. Phys. Chem. B* **2006**, *110*, 10401-10410

at.%				η (mV) at *J* mA/cm2		
Ni	Fe	Co	Ce	*J* =1	J=10	J=19
49	49	0	0	363	415	428
49	47	3	0	360	412	425
49	43	7	0	359	410	422
49	40	10	0	359	410	422
49	30	20	0	358	407	421
49	27	23	0	358	406	419
49	23	27	0	358	406	426
49	20	30	0	359	409	422
49	16	32	0	360	411	427
49	12	36	0	362	415	430
49	10	40	0	365	418	433
49	7	43	0	371	425	441
49	3	47	0	350	404	414
49	0	49	0	351	410	425
47	49	3	0	348	398	410
47	47	7	0	351	398	409
47	43	10	0	351	398	410
47	40	12	0	350	397	406
47	36	16	0	349	396	404
47	32	20	0	348	396	404
47	30	23	0	347	397	405
47	27	27	0	348	396	403
47	23	30	0	346	395	402
47	20	32	0	346	396	404
47	16	36	0	348	397	407
47	12	40	0	348	399	411
47	10	43	0	349	401	411
47	7	47	0	353	408	413
47	3	49	0	357	410	421
52	43	0	3	347	395	416
52	40	3	3	345	393	413
52	36	7	3	345	394	412
52	32	10	3	346	394	412
52	30	12	3	346	393	410
52	23	20	3	347	391	404
52	20	23	3	346	394	402
52	12	30	3	346	396	393
52	7	36	3	346	394	410
52	3	40	3	346	399	414
52	0	43	3	351	416	430
49	43	3	3	350	404	408
49	40	7	3	349	400	406
49	36	10	3	349	399	407
49	32	12	3	348	396	410

at.%				η (mV) at *J* mA/cm2		
Ni	Fe	Co	Ce	*J* =1	J=10	J=19
40	23	20	16	334	388	397
40	20	23	16	337	387	397
40	16	27	16	336	387	399
40	12	30	16	335	387	401
40	10	32	16	335	389	412
40	7	36	16	335	392	411
40	3	40	16	336	399	421
36	40	7	16	340	393	410
36	36	10	16	343	412	416
36	32	12	16	336	392	395
36	27	20	16	332	383	398
36	23	23	16	331	381	399
36	20	27	16	330	380	399
36	16	30	16	328	380	400
36	12	32	16	329	380	405
36	10	36	16	327	381	410
36	7	40	16	326	383	415
36	3	43	16	328	390	425
43	36	0	20	337	383	401
43	32	3	20	336	385	399
43	30	7	20	331	381	395
43	27	10	20	330	381	392
43	23	12	20	328	380	397
43	20	16	20	328	381	386
43	16	20	20	329	382	404
43	12	23	20	327	382	397
43	10	27	20	326	383	406
43	3	32	20	328	392	415
43	0	36	20	331	398	420
40	36	3	20	336	388	401
40	32	7	20	337	385	387
40	30	10	20	333	384	391
40	27	12	20	331	383	392
40	23	16	20	329	382	390
40	20	20	20	329	383	393
40	16	23	20	329	384	397
40	12	27	20	333	385	398
40	10	30	20	333	386	400
40	7	32	20	332	388	406
40	3	36	20	331	393	415
40	0	40	20	332	397	422
36	36	7	20	336	388	406
36	32	10	20	336	387	399
36	30	12	20	333	386	397

at.%				η (mV) at *J* mA/cm2		
Ni	Fe	Co	Ce	*J* =1	J=10	J=19
27	27	7	40	319	387	393
27	23	10	40	317	386	403
27	20	12	40	317	381	401
27	16	16	40	315	383	393
27	12	20	40	313	378	391
27	10	23	40	307	377	400
27	7	27	40	306	384	400
27	3	30	40	303	377	409
23	27	10	40	307	391	410
23	23	12	40	313	366	402
23	20	16	40	322	391	401
23	16	20	40	322	391	406
23	10	27	40	313	375	418
30	23	3	43	322	378	399
30	20	7	43	317	376	399
30	16	10	43	314	374	399
30	12	12	43	310	372	403
30	10	16	43	308	370	403
30	7	20	43	318	375	408
30	3	23	43	319	376	413
30	0	27	43	320	382	424
27	23	7	43	316	376	403
27	20	10	43	313	374	403
27	16	12	43	309	372	405
27	12	16	43	311	371	406
27	10	20	43	324	377	406
27	7	23	43	319	377	411
27	3	27	43	317	376	415
27	0	30	43	317	379	418
23	27	7	43	321	383	410
23	23	10	43	311	371	392
23	20	12	43	311	372	394
23	16	16	43	306	368	397
23	12	20	43	316	372	396
23	10	23	43	315	372	397
23	7	27	43	314	371	406
23	3	30	43	313	371	408
20	23	12	43	309	371	395
20	12	23	43	319	374	396
20	3	32	43	313	373	408
27	20	7	47	327	386	394
27	16	10	47	318	379	397
27	12	12	47	313	375	400
27	10	16	47	309	371	395

49	30	16	3	346	398	407
49	27	20	3	345	396	405
49	23	23	3	346	404	404
49	20	27	3	345	397	404
49	16	30	3	347	398	403
49	12	32	3	349	397	410
49	10	36	3	349	400	412
49	7	40	3	345	400	409
49	3	43	3	344	404	416
49	0	47	3	347	411	430
47	47	3	3	348	403	412
47	43	7	3	349	399	413
47	36	12	3	348	399	409
47	32	16	3	348	403	412
47	30	20	3	350	397	411
47	27	23	3	350	402	408
47	23	27	3	349	406	408
47	20	30	3	349	401	409
47	16	32	3	337	382	389
47	10	40	3	339	390	386
47	7	43	3	339	391	400
47	3	47	3	339	395	407
43	49	3	3	347	405	411
43	43	10	3	345	390	400
43	40	12	3	346	390	396
43	36	16	3	345	388	397
43	30	23	3	344	399	398
43	27	27	3	344	397	397
43	23	30	3	340	398	397
43	20	32	3	341	400	396
43	16	36	3	341	389	397
43	12	40	3	340	403	395
43	7	47	3	338	407	405
43	3	49	3	345	424	472
49	43	0	7	342	390	392
49	40	3	7	342	391	400
49	36	7	7	340	391	403
49	32	10	7	340	390	394
49	30	12	7	338	389	396
49	23	20	7	344	388	402
49	20	23	7	342	387	395
49	16	27	7	342	388	395
49	12	30	7	339	389	389
49	10	32	7	339	390	400
49	7	36	7	340	392	398
49	3	40	7	343	398	411
47	43	3	7	345	394	404

36	27	16	20	335	384	396
36	23	20	20	333	384	396
36	20	23	20	333	384	396
36	16	27	20	332	385	398
36	12	30	20	332	386	409
36	10	32	20	331	386	406
36	7	36	20	330	389	407
36	3	40	20	332	395	420
32	32	12	20	336	387	399
32	23	23	20	333	386	399
32	12	32	20	333	390	409
32	3	43	20	334	402	424
43	27	7	23	333	386	401
43	7	27	23	333	395	420
40	32	3	23	340	391	405
40	30	7	23	335	389	400
40	27	10	23	335	390	400
40	23	12	23	335	387	399
40	20	16	23	334	387	399
40	16	20	23	332	387	403
40	12	23	23	335	390	408
40	10	27	23	334	392	414
40	7	30	23	334	397	421
40	3	32	23	334	400	429
40	0	36	23	332	398	435
36	36	3	23	342	393	404
36	32	7	23	341	391	403
36	30	10	23	330	376	396
36	27	12	23	331	381	392
36	23	16	23	326	378	388
36	20	20	23	325	379	392
36	16	23	23	325	379	399
36	12	27	23	324	380	402
36	10	30	23	326	384	410
36	7	32	23	329	388	412
36	3	36	23	332	390	419
32	36	7	23	331	385	399
32	32	10	23	332	384	399
32	30	12	23	330	383	395
32	27	16	23	328	382	394
32	23	20	23	327	381	394
32	20	23	23	327	383	398
32	16	27	23	327	383	397
32	12	30	23	330	384	401
32	10	32	23	332	387	412
32	7	36	23	331	388	408
32	3	40	23	331	394	403

27	7	20	47	306	371	403
27	3	23	47	304	369	406
27	0	27	47	317	377	410
23	23	7	47	324	386	399
23	20	10	47	318	405	405
23	16	12	47	317	390	406
23	12	16	47	314	389	403
23	10	20	47	310	371	413
23	7	23	47	303	363	403
20	23	10	47	317	385	404
20	20	12	47	314	380	403
20	16	16	47	310	379	400
20	12	20	47	306	370	401
20	10	23	47	304	367	403
20	7	27	47	314	373	404
20	3	30	47	311	373	409
27	20	3	49	331	398	407
27	16	7	49	327	396	413
27	12	10	49	315	389	404
27	10	12	49	308	377	404
27	7	16	49	303	372	408
27	3	20	49	296	370	412
27	0	23	49	298	370	412
23	20	7	49	304	379	404
23	16	10	49	306	372	405
23	12	12	49	298	362	406
23	10	16	49	298	362	407
23	7	20	49	299	369	409
23	3	23	49	294	365	409
23	0	27	49	319	377	405
20	23	7	49	329	389	400
20	20	10	49	322	383	407
20	16	12	49	316	380	397
20	12	16	49	313	375	404
20	10	20	49	308	370	404
20	7	23	49	303	368	410
20	3	27	49	301	367	404
16	23	10	49	325	384	407
16	7	27	49	303	366	399
23	7	16	52	311	372	401
23	3	20	52	296	382	400
23	0	23	52	298	387	401
20	20	7	52	311	382	406
20	16	10	52	297	370	406
20	12	12	52	301	380	404
20	10	16	52	315	377	403
20	3	23	52	303	385	404

47	40	7	7	343	390	398
47	36	10	7	344	398	399
47	32	12	7	342	396	396
47	30	16	7	342	396	397
47	27	20	7	340	391	399
47	23	23	7	339	392	397
47	20	27	7	337	392	386
47	16	30	7	340	390	385
47	12	32	7	337	389	395
47	10	36	7	337	391	399
47	7	40	7	343	394	399
47	3	43	7	343	400	413
47	0	47	7	343	403	418
43	47	3	7	346	395	409
43	43	7	7	344	395	403
43	40	10	7	344	394	401
43	36	12	7	344	391	402
43	32	16	7	344	392	407
43	30	20	7	340	391	399
43	27	23	7	342	392	395
43	23	27	7	342	392	398
43	20	30	7	344	392	398
43	16	32	7	342	392	397
43	12	36	7	343	393	403
43	10	40	7	344	397	407
43	7	43	7	342	399	409
49	40	0	10	344	402	412
49	36	3	10	344	396	408
49	32	7	10	348	391	405
49	30	10	10	346	391	403
49	27	12	10	344	390	400
49	23	16	10	343	389	398
49	20	20	10	342	392	399
49	16	23	10	341	392	400
49	12	27	10	341	395	404
49	10	30	10	345	395	405
49	7	32	10	331	384	405
49	3	36	10	335	395	420
49	0	40	10	335	397	434
47	43	0	10	341	392	409
47	40	3	10	339	389	407
47	36	7	10	337	388	404
47	32	10	10	338	391	402
47	30	12	10	337	389	404
47	27	16	10	339	385	403
47	23	20	10	338	387	404
47	20	23	10	336	387	400

40	30	3	27	332	384	401
40	27	7	27	329	384	401
40	23	10	27	327	382	402
40	20	12	27	327	383	401
40	16	16	27	323	378	404
40	12	20	27	323	383	411
40	10	23	27	321	377	412
40	7	27	27	323	389	417
40	3	30	27	320	392	423
40	0	32	27	325	390	432
36	32	3	27	332	385	409
36	30	7	27	333	382	398
36	27	10	27	321	382	400
36	23	12	27	327	375	403
36	20	16	27	322	381	404
36	16	20	27	319	382	408
36	12	23	27	318	383	411
36	10	27	27	326	383	414
36	7	30	27	326	386	419
36	3	32	27	331	392	426
36	0	36	27	326	393	428
32	32	7	27	330	384	405
32	30	10	27	330	384	404
32	27	12	27	324	383	405
32	23	16	27	325	383	402
32	20	20	27	321	383	402
32	16	23	27	329	382	403
32	12	27	27	325	380	407
32	10	30	27	322	385	409
32	7	32	27	331	389	416
32	3	36	27	326	389	431
30	36	7	27	322	383	404
30	32	10	27	324	385	404
30	30	12	27	322	383	406
30	27	16	27	330	383	403
30	23	20	27	329	378	402
30	20	23	27	330	384	402
30	16	27	27	328	383	404
30	12	30	27	329	385	409
30	10	32	27	328	383	414
30	7	36	27	331	388	420
36	30	3	30	331	384	397
36	27	7	30	330	384	396
36	23	10	30	328	384	403
36	20	12	30	334	385	393
36	16	16	30	329	382	396
36	12	20	30	329	383	397

16	20	10	52	311	389	421
16	16	12	52	329	394	413
16	12	16	52	326	389	408
16	10	20	52	323	385	405
16	7	23	52	322	391	405
16	3	27	52	315	393	406
23	12	7	56	309	388	415
23	10	10	56	329	388	415
23	7	12	56	324	385	412
23	3	16	56	322	382	413
23	0	20	56	320	385	417
20	16	7	56	314	387	414
20	12	10	56	310	382	414
20	10	12	56	327	390	416
20	7	16	56	325	385	413
20	3	20	56	318	380	414
20	0	23	56	313	376	409
16	16	10	56	312	385	419
16	12	12	56	335	398	419
16	10	16	56	325	382	413
16	7	20	56	323	383	423
12	20	10	56	316	390	417
12	16	12	56	311	383	412
12	12	16	56	323	386	414
12	7	23	56	313	375	419
20	7	12	60	313	391	407
20	3	16	60	307	383	402
16	16	7	60	344	425	425
16	12	10	60	336	409	419
16	10	12	60	322	395	411
16	7	16	60	315	388	404
16	3	20	60	309	377	400
16	0	23	60	305	371	404
12	16	10	60	336	422	423
12	12	12	60	329	402	420
12	10	16	60	321	390	410
12	7	20	60	313	379	411
12	3	23	60	319	387	405
20	10	7	63	337	405	420
20	7	10	63	326	395	420
20	3	12	63	316	382	415
20	0	16	63	310	373	409
16	12	7	63	345	410	423
16	10	10	63	337	402	421
16	3	16	63	313	379	409
16	0	20	63	311	386	403
12	12	10	63	333	413	425

47	16	27	10	335	385	399
47	12	30	10	334	387	401
47	10	32	10	335	388	404
47	7	36	10	336	399	409
47	3	40	10	335	403	415
47	0	43	10	337	409	426
43	43	3	10	342	401	405
43	40	7	10	344	398	404
43	36	10	10	343	397	401
43	32	12	10	342	392	398
43	30	16	10	340	392	397
43	27	20	10	339	393	399
43	23	23	10	337	393	395
43	20	27	10	336	385	395
43	16	30	10	336	395	398
43	12	32	10	336	396	400
43	10	36	10	339	401	409
43	7	40	10	338	407	415
43	3	43	10	338	412	430
40	40	10	10	346	403	408
40	36	12	10	343	398	406
40	32	16	10	341	392	408
40	30	20	10	341	401	407
40	27	23	10	338	388	407
40	23	27	10	337	388	409
40	20	30	10	343	404	412
40	16	32	10	344	406	408
40	12	36	10	338	398	410
40	10	40	10	342	398	411
40	7	43	10	342	400	418
40	3	47	10	342	403	429
47	40	0	12	340	393	401
47	36	3	12	339	391	398
47	32	7	12	343	387	398
47	30	10	12	343	388	401
47	27	12	12	341	389	396
47	23	16	12	342	390	396
47	20	20	12	338	388	396
47	16	23	12	338	389	397
47	12	27	12	337	389	398
47	10	30	12	336	390	402
47	7	32	12	340	396	417
47	3	36	12	343	403	420
47	0	40	12	339	404	423
43	40	3	12	342	401	404
43	36	7	12	339	389	402
43	32	10	12	339	397	402

36	10	23	30	328	384	407
36	7	27	30	325	386	412
36	3	30	30	324	390	412
36	0	32	30	329	394	435
32	30	7	30	335	387	401
32	27	10	30	333	385	400
32	23	12	30	330	383	399
32	20	16	30	328	385	400
32	16	20	30	328	383	408
32	12	23	30	316	375	402
32	10	27	30	318	376	406
32	7	30	30	315	379	411
32	3	32	30	317	382	421
30	32	7	30	329	378	401
30	30	10	30	325	377	403
30	27	12	30	322	376	402
30	23	16	30	321	375	406
30	20	20	30	319	374	405
30	16	23	30	317	375	406
30	12	27	30	319	376	407
30	10	30	30	319	377	415
30	7	32	30	317	380	422
36	27	3	32	327	383	403
36	23	7	32	327	382	403
36	20	10	32	327	384	403
36	16	12	32	329	384	406
36	12	16	32	321	372	399
36	10	20	32	322	380	403
36	7	23	32	316	375	408
36	3	27	32	316	379	415
36	0	30	32	315	380	418
32	30	3	32	322	376	397
32	27	7	32	326	375	393
32	23	10	32	323	374	393
32	20	12	32	320	374	394
32	16	16	32	318	374	397
32	12	20	32	317	374	396
32	10	23	32	314	374	404
32	7	27	32	316	376	414
32	3	30	32	315	379	423
32	0	32	32	315	381	421
30	30	7	32	326	377	394
30	27	10	32	324	376	397
30	23	12	32	323	376	398
30	20	16	32	319	375	398
30	16	20	32	317	376	396
30	12	23	32	315	375	401

12	7	16	63	323	397	410
12	3	20	63	315	387	405
10	16	10	63	340	420	435
10	12	12	63	319	397	428
10	10	16	63	312	385	419
10	7	20	63	323	389	413
10	3	23	63	317	381	406
16	10	7	67	328	401	414
16	7	10	67	314	388	414
16	3	12	67	304	375	412
16	0	16	67	314	377	404
12	10	10	67	331	406	423
12	7	12	67	315	390	415
12	3	16	67	317	384	404
12	0	20	67	313	376	400
10	12	10	67	342	409	420
10	10	12	67	329	403	419
10	7	16	67	315	388	410
10	3	20	67	307	375	402
7	12	12	67	335	416	432
16	3	10	70	315	396	417
16	0	12	70	307	380	403
12	10	7	70	346	422	430
12	7	10	70	334	415	437
12	3	12	70	315	395	409
12	0	16	70	319	390	404
10	10	10	70	344	415	427
10	7	12	70	335	409	438
10	3	16	70	319	392	422
7	12	10	70	345	418	442
7	10	12	70	339	417	441
7	7	16	70	324	403	439
7	3	20	70	308	382	420
12	7	7	72	346	423	442
12	3	10	72	328	409	444
12	0	12	72	315	389	427
10	7	10	72	341	419	442
10	3	12	72	320	402	434
10	0	16	72	308	378	411
7	10	10	72	351	432	456
7	7	12	72	333	418	451
7	3	16	72	315	393	429
12	3	7	76	337	428	462
12	0	10	76	321	404	442
10	3	10	76	338	425	447
10	0	12	76	327	405	444
7	7	10	76	356	432	457

43	30	12	12	341	401	408
43	27	16	12	339	398	400
43	23	20	12	341	397	400
43	20	23	12	340	397	399
43	16	27	12	338	399	400
43	12	30	12	337	388	404
43	10	32	12	336	395	408
43	7	36	12	340	409	420
43	3	40	12	330	393	420
43	0	43	12	335	401	441
40	43	3	12	339	398	407
40	40	7	12	338	394	405
40	36	10	12	336	392	401
40	32	12	12	336	391	403
40	30	16	12	335	391	405
40	27	20	12	334	390	405
40	23	23	12	333	386	404
40	20	27	12	331	390	403
40	16	30	12	328	392	402
40	12	32	12	326	387	406
40	10	36	12	329	386	407
40	7	40	12	336	395	413
40	3	43	12	330	398	424
36	36	12	12	331	396	404
36	32	16	12	335	386	404
36	16	32	12	338	397	407
36	12	36	12	337	397	408
47	30	7	16	338	396	391
47	10	27	16	331	385	395
47	7	30	16	329	386	400
43	36	3	16	338	389	397
43	32	7	16	344	389	401
43	30	10	16	342	389	395
43	27	12	16	336	386	395
43	23	16	16	333	385	394
43	20	20	16	331	385	397
43	16	23	16	331	385	398
43	12	27	16	331	386	400
43	10	30	16	333	389	411
43	7	32	16	337	389	403
43	3	36	16	334	393	411
43	0	40	16	337	400	416
40	40	3	16	339	391	400
40	36	7	16	336	389	398
40	32	10	16	338	389	405
40	30	12	16	338	390	399
30	10	27	32	316	378	406
30	7	30	32	315	380	413
30	3	32	32	325	387	416
27	32	7	32	326	387	398
27	30	10	32	324	385	397
27	27	12	32	322	384	393
27	20	20	32	319	378	398
27	16	23	32	319	378	404
27	12	27	32	318	379	402
27	10	30	32	325	382	404
27	7	32	32	324	384	409
27	3	36	32	325	385	415
32	27	3	36	320	379	397
32	23	7	36	318	378	397
32	20	10	36	317	378	399
32	16	12	36	324	380	399
32	10	20	36	320	415	422
32	7	23	36	317	384	423
32	3	27	36	316	387	426
30	27	7	36	320	383	408
30	23	10	36	326	378	410
30	20	12	36	324	376	407
30	16	16	36	322	376	411
30	12	20	36	318	375	411
30	10	23	36	317	375	409
30	7	27	36	314	374	413
27	30	7	36	330	381	401
27	27	10	36	328	378	399
27	23	12	36	324	377	400
27	20	16	36	323	377	398
27	16	20	36	323	378	407
27	12	23	36	317	373	405
27	10	27	36	315	374	408
27	7	30	36	309	373	413
32	23	3	40	321	377	397
32	20	7	40	318	375	397
32	16	10	40	315	374	393
32	12	12	40	313	373	394
32	10	16	40	312	373	398
32	7	20	40	320	376	402
32	3	23	40	321	378	414
32	0	27	40	317	378	407
30	23	7	40	317	388	395
30	16	12	40	314	384	393
30	12	16	40	314	384	394
30	10	20	40	321	386	401
7	3	12	76	333	418	437
3	7	12	76	362	443	472
3	3	16	76	337	425	447
10	3	7	80	349	446	461
10	0	10	80	337	428	448
7	3	10	80	349	445	454
3	3	12	80	354	446	459
0	7	12	80	381	466	479
0	3	16	80	361	456	464
7	0	10	83	347	453	476
3	3	10	83	375	465	493
0	3	12	83	376	461	486
7	0	7	87	374	479	496
3	0	10	87	378	477	502